International Conference on Space Optics—ICSO 2018

Chania, Greece

9–12 October 2018

Edited by Zoran Sodnik, Nikos Karafolas, and Bruno Cugny

Cheops optical calibration campaign

Bruno Chazelas

Adrien Deline

F. Wildi

Mirsad Sarajlic

et al.

International Conference on Space Optics — ICSO 2018, edited by Zoran Sodnik, Nikos Karafolas, Bruno Cugny, Proc. of SPIE Vol. 11180, 111802U · © 2018 ESA and CNES · CCC code: 0277-786X/18/$18 · doi: 10.1117/12.2536021

Cheops optical calibration campaign

Bruno Chazelas[a], Adrien Deline[a], Francois Wildi[a], Mirsad Sarajlic[b], Michaël Sordet[a], Thibault Kuntzer[a]
[a]Geneva Observatory, University of Geneva, Maillettes 51, 1290 Sauverny, Switzerland
[b]Swiss Optics Systems, Yverdon, Switzerland

ABSTRACT

The ESA S mission CHEOPS relies on a photometer for the precise measurement of the radius of exoplanet. This information is essential to better constrain the nature and structure of exoplanets. The CHEOPS payload is a small defocused telescope of 32-cm aperture that went through its characterization campaign in the first quarter of 2018. We report here on the techniques developed for the calibration campaign and the results of the obtained. In particular we have measured high-precision color-dependent flat fields, measured the characteristics of the detection chain, gain, full-well capacity, read-out noise, measured the instrument distortion and explored the PSF behavior across the field. The end-to-end photometric stability of the instrument has also been measured and we will be reporting on the results and the difficulties that have come up while attempting this very difficult measurement, for which sophisticated design and methods were developed.
Keywords: CHEOPS, exoplanet, transit, photometry

1. INTRODUCTION

ESA S mission CHEOPS[1], aims to improve our knowledge, of exoplanet radii through the high-precision photometric monitoring of their transits. This will allow to better constrain the density of these planets and help to better distinguish between rocky planets, gaseous giants and all the possible intermediate zoo of planets. The satellite has access to a large fraction of the sky, thus it will be able to characterize a large part of the transiting planets, already known and to be discovered by the next exoplanet discovering machines such as TESS[2] and PLATO[3], or ground based detection surveys such a NGTS[4], SPECULOOS[5] and others.

CHEOPS payload is a simple defocused 32-cm telescope. In order to fulfill the ambitious science goals of the mission, it has to reach an absolute photometric precision of 20 ppm. The focal plane is a CCD-47-20 from E2V. In order to ensure this performance level, it is necessary to maintain the detector temperature to a stability level around 10 mK, and the detector bias voltage stability to a few microvolts. The pointing of the instrument is done with reaction wheels. Its stability cannot be better than a few arcsecond. As a consequence, the PSF of the instrument will move on the detector. It is thus necessary to measure the Flat field of the instrument with 0.1% precision in order to be able to recover the 20-ppm precision required. Only a 200x200 portion of this array will be transmitted to the ground, however we have performed calibration on the full area of the CCD as the possibility to move the scientific window is a part of the instrument redundancy. It will in particular allow to avoid hot pixels that will appear in orbit.

After a successful CCD test[6] campaign, a test bench[7] to perform the needed instrument calibration and to test the instrument performances has been built. We report here the results of this calibration campaign. We could perform the following measurements and characterizations:

- Measurement of the Bias / Dark / Hot pixel determinations.
- Measurement of the Gain / Linearity / Full-well capacity
- Measurement of color-dependent flat fields.
- An assessment of the photometric performance of the instrument

2. BIAS – DARK – LINEARITY MEASUREMENTS

The calibrations campaign took place at the beginning of 2018. It has been the first time the full instrument was assembled. The detector chain has been characterized with the real flight electronics. The measurements were performed in a similar fashion as in our CCD tests[6]. Results are shown in the Table 1. Two reading speeds are implemented, 230 kHz for bright stars and 100 kHz for faint stars.

Table 1 Summary of the measured characteristics of the CHEOPS instrument. Two reading speeds are available on board, a fast mode for bright stars at 230 kHz and a slow reading mode for the faint stars at 100 kHz.

Characteristics	**Value**
RON Nominal 230 kHz	7.2 e^-
RON Nominal 100 kHz	3.5 e^-
RON redundant 230 kHz	7.3 e^-
RON redundant 100 kHz	3.4 e^-
Bias oscillation	0.4 e^- at 230 kHz, none at 100 kHz
Gain Nominal 230 kHz	0.511 +/- 0.003
Gain Nominal 100 kHz	0.511 +/- 0.003
Gain Redundant 230 kHz	0.507 +/- 0.003
Gain Redundant 100 kHz	---
Gain temperature sensitivity	-900 ppm/K
Non-linearity amplitude	1.2 % (from 10^4 to $1.1x10^5$ e^-)
Dark	0.056 e^-/s
Warm pixels (> 5 e^-/s)	7 pixels
Full Well	114 ke^- - 121 ke^-

The way the CCD saturate has been a surprise. During the CCD tests[6], the full well of the CCD was reached in average at the same level all across the CCD.

With the flight electronics, the situation has dramatically changed, the full well seem to be reached sooner in the center of the CCD. Blooming starts in the center before than on the borders. In addition, before the saturation is reached, a fix pattern noise appears, lowering a bit more the available dynamic. The origin of this fix pattern noise is unknown. It had already been seen on ULTRACAM[8] with the same E2V CCD and called peppering effect. Figure 1 shows the map of the usable dynamic on the CCD.

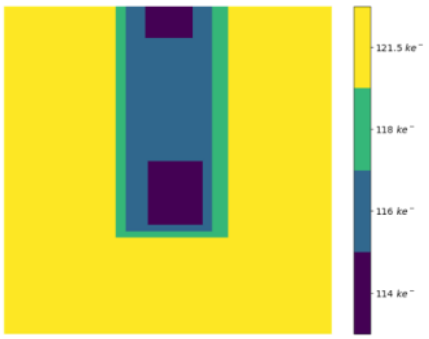

Figure 1 Image showing the dynamic range of the CCD (in electrons. The darkest areas show at which level the early saturation starts and how it spreads upward. This reduces the dynamic range as indicated by the color bar. This image was made manually and the scale values are conservative.

The consequence of this effect, and the fact that the reading electronics gain is slightly too high, makes it very difficult to do photometry with saturated stars, which would have been a desirable possibility of the system.

The gain is identical at both reading speeds, and as far we could test the same in science window mode. The linearity for the fast reading mode is shown on Figure 2.

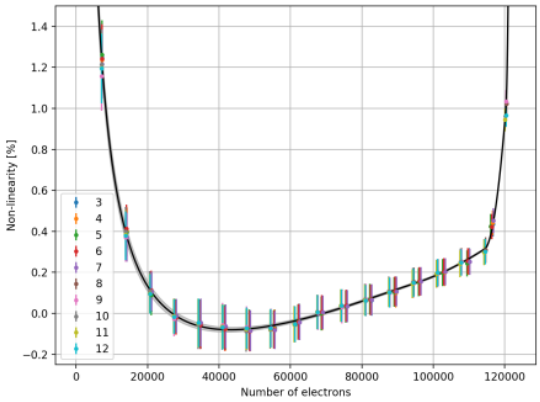

Figure 2 Non-linearity curve for both channels at a read-out frequency of 230kHz. The color code (numbers from 3 to 12) represents different measurement conditions (temperatures and channels).

3. FLAT-FIELDS

One of the most important calibration to perform was the flat fielding of the instrument. As the stellar spectrums vary substantially we set out to build high-precision color-dependent flat-fields measurements. For this we used an integrating sphere at the focus of the calibration set-up[7]. To have a final precision of 0.1% many steps were necessary.

While this integrating sphere had a diameter of 280 mm, and a port of only 20 mm, we could measure a radial non-uniformity of its illumination. We measured this using a monochromator and a dedicated scanning set-up to make a 2D map of the sphere illumination, at the required precision. We could model non-uniformity with a radial function (see Figure 3). Doing successfully this measurement, that lasted a week, and having consistent result proved the reliability of our set-up. In order to be able to apply this correction to the images we used a mechanical reference so that it was possible to calculate the correction in the pixel space.

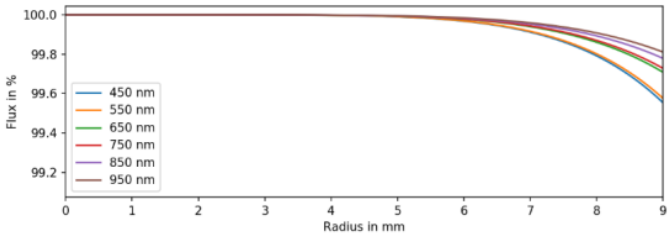

Figure 3 Model of the sphere non-uniformity radial dependence as a function of wavelength, the integrating sphere has a diameter of 280 mm and the output port is 20 mm in diameter. The radius here is reported in the port frame.

The optics of the telescope have a non-negligible level of distortion. This has photometric consequences on the flat-field measured. There is an excess of light on the border of the image, because of barrel distortion. It is necessary to characterize properly the distortion because when doing aperture photometry with a star (a point source), the flat-field need to be debiased as the detector is not actually more sensitive on the border.

Distortion has been measured using a standard high precision grid of point stamped on a glass plate. It has been installed in front of the integrating sphere. With this measurement it was possible to determine the optical center of the field and a second order model of the distortion.

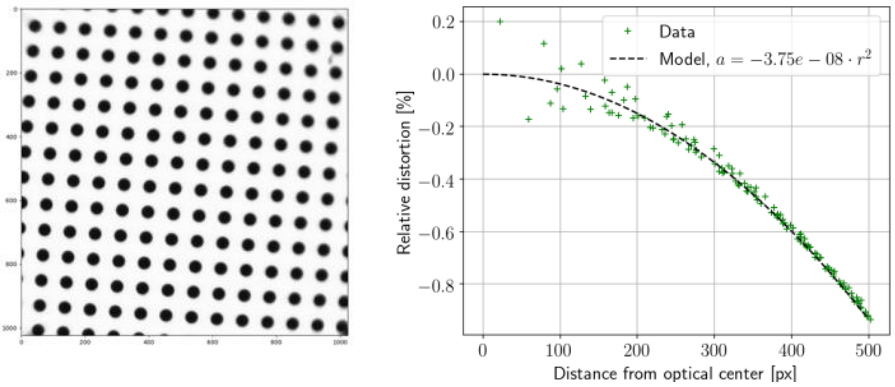

Figure 4 *Left*, image of the grid with the instrument. *Right*, distortion measurement and wavelength at 985 nm.

The pixel response non-uniformity of a CCD varies significantly with wavelength[6]. To improve the final precision of the flat-field corrections we made a color dependent measurement. We measured flat-fields using a mix of standard photometric filters (Johnson UBVRI filters) and monochromator defined wavelengths (there are 43 wavelengths from 440 nm to 950 nm). It is thus possible to reproduce smooth stellar spectrums. It has also been necessary to calibrate the spectrum of the white source that was used, the transmission of the instrument and the Quantum Efficiency of the detector.

A particular care has been taken to understand the fringing of the detector. Using the monochromator at a high sampling in wavelength it has been possible to determine the frequency of the wavelength periodicity of the fringe contrast inversion. This allows to estimate the systematic error one does in sampling the flat field in the fringing region. We could find a periodicity of 4.55 nm. Thus, in order to limit the systematic errors due to fringing it is necessary to integrate over the full I band (see Figure 5).

In order to prove that we could recombine the flat field we could make a measurement using a tungsten lamp as a source. Once its spectrum calibrated it is possible to determine the combination of flat-fields necessary to approximate at best the lamp spectrum (see Figure 5). If we compare the measured flat-field (Figure 6) and the recombined one the error is well below 0.1% and very near to the photonic limit.

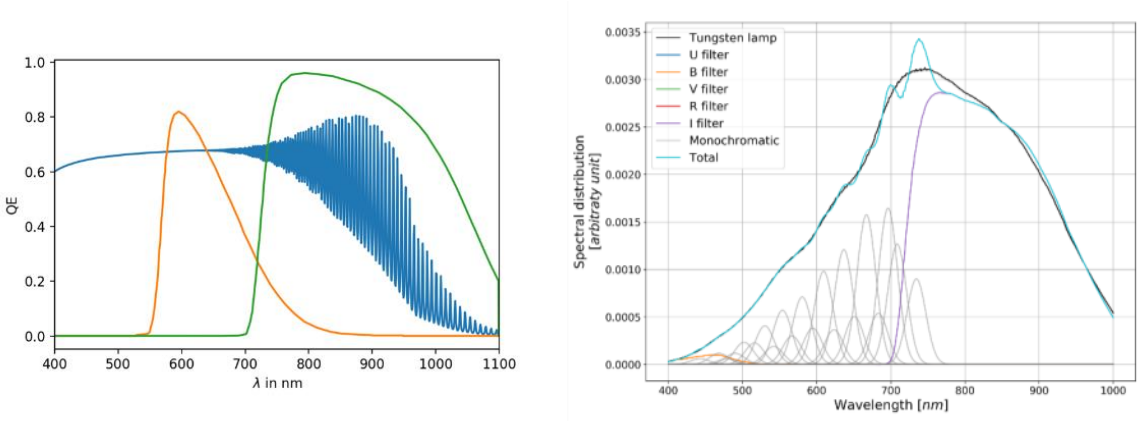

Figure 5 *Left*, the blue curve is a model of the QE of the CCD including the fringing, The two other curves are the R and I Johnson filters. *Right*, test of the spectral recombination of the flat fields. Graph showing the Tungsten lamp spectrum used as reference (black). The U, B ,V,R ,I (Johnson filters) and monochromatic spectral distributions have been weighted to best fit the reference profile. The sum of all these profiles is the cyan curve called "Total". The U,V and R filters are not visible on the figure because their coefficients are nil. This is due to the fact that the U filter is too blue to fit the black curve, and that the V and R filters are compensated by the monochromatic profiles.

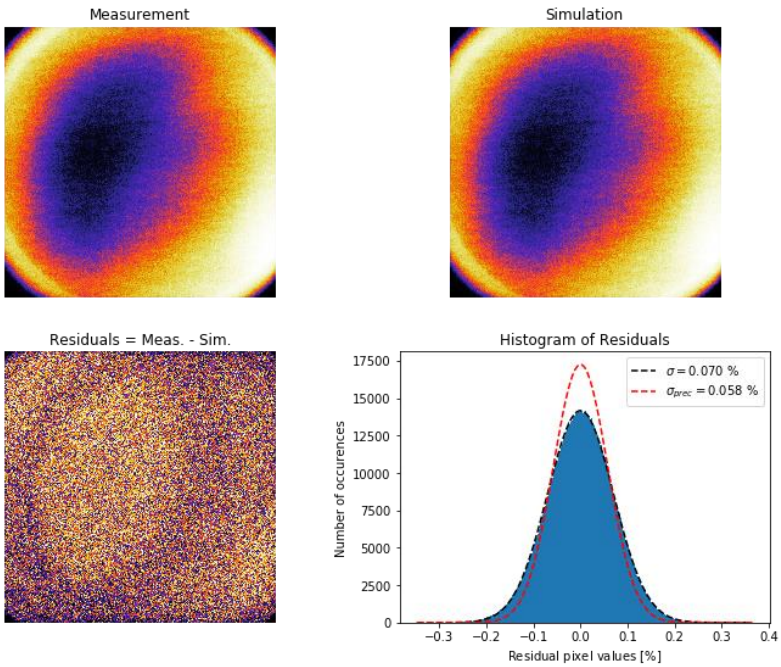

Figure 6 Results of the flat field combination for the Tungsten lamp. The upper left image shows the measured flat field. The upper right image shows a synthesized flat field, which is a weighted average of the monochromatic and Johnsons filters measurements. The lower left image is the residuals of the two top images. The lower right graph shows the histogram of the residuals in blue, with a standard deviation of 0.070%. The two dashed lines are plotted for visualization purposes: the black one is a Gaussian distribution with the same dispersion as the residuals, and the red one represents what could be reached if we were only limited by the noise (0.058%).

4. PSF MEASUREMENTS

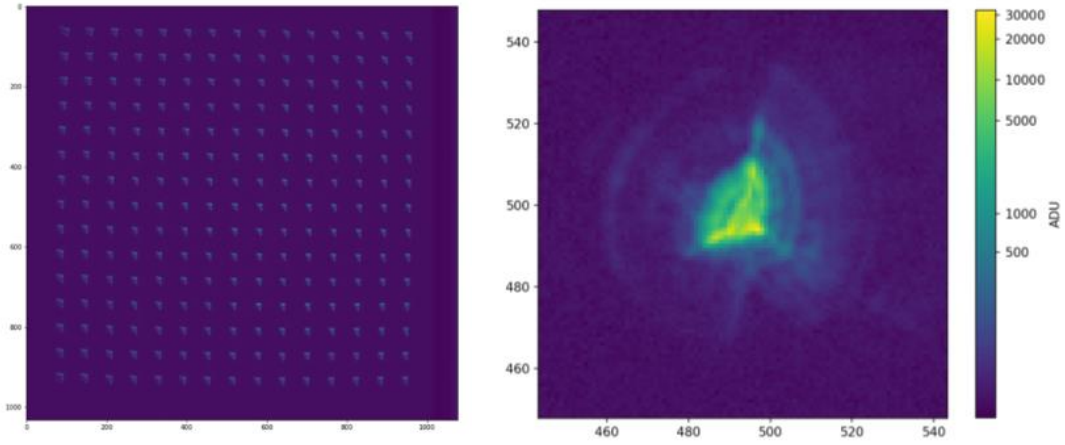

Figure 7 *Left* a composite image showing the PSF evolution over the full field of view of the instrument, *Right* the PSF measured in the center of the field.

PSF measurements were performed using the test bench in point source mode. It allows to check that the optical alignment of the telescope is in line with expectations. The measurements suffer from some issues: the pupil uniformity of the test bench was suboptimal (12% center to border), the optical quality of the bench was by design around λ/3, and the telescope was pointing horizontally in the test chamber, thus the gravity affect the aberrations of the PSF. Only in-flight measured PSF could be used to do any kind of scientific data analysis.

In the center of the field, the PSF encircled energy radius at 90% is 12.8 ±0.3 pixels at 680 nm. The PSF, in one exposure, can hold ~ 4.5 10^6 e^- (this is an order of magnitude). The low-flux large-scale diffraction halo that can be seen on the Figure 7 is probably due to the mid-spatial frequency wavefront errors that are present on the primary mirror and will probably remain in space.

5. PHOTOMETRIC STABILITY

We had set-up[7] to prove experimentally the end-to-end photometric stability of the instrument. In order to perform such a measurement, we have developed a Super Stable Source[9] (SSS), a closed loop system to stabilize the source of the test bench to the ppm level. The full test would have been to illuminate the instrument with a star like source, and thanks to precise control of the field and the pupil alignment of the test bench, the test bench induced photometric variations would have remained small enough to show the instrument performances. The plan was also to perform the test adding jitter to the PSF position, and slowly changing the temperature of the telescope to mimic the in-orbit environment. Because of time constraints we had to limit the number of tests and the full end-to-end measurement was not performed. It has been however possible to make some long-term stability measurement using an integrating sphere as a source. Because of issues that had not been understood at the moment of the measurement we used the SSS in open loop, but we recorded the photometric control signal as well as some environmental data. The instrument house-keeping data were also recorded. It is thus possible to detrend the data acquired with the instrument from most of the test bench induced photometric variations.

The first approach to check the stability of the instrument is to check the stability of the CCD temperature, and its reading electronics. It is also necessary to check the stability of the bias voltages. The Table 2 below summarize the performances and the requirements. Everything is well in the requirement.

Table 2 Stability of the different electrical and thermal parameter of the instrument detector.

	Measured	**Predicted Effect on photometry**
CCD temperature	1.2 mK rms over (27 h)	1.79 ppm
FEE temperature	0.5 mK rms over (27 h)	0.75 ppm
ADC temperature	0.7 mK rms over (27 h)	1.05 ppm
VOD (bias voltage)	34 µV rms over (27 h)	1.2 ppm
VRD (bias voltage)	25 µV rms over (27 h)	0.23 ppm
VOG (bias voltage)	21 µV rms over (27 h)	0.17 ppm
VSS (bias voltage)	9 µV rms over (27 h)	0.26 ppm

On Figure 8 one can see the nearly exact correspondence between the photometric data from the instrument and the one from the reference photometer. However, once the ratio of the two measurements done, there is still a low frequency structure. This structure is correlated with the temperature in the lab.

This can be explained by an unfortunate property of the optical fiber that was used during the measurement. We did not realize when we chose the fiber that it had a double cladding. It means that the fiber has a double guiding structure and that light is transported not only in the core but also in the first cladding. More over the second guiding structure has an aperture that is twice as big as the one of the core guiding structure. The light used for the reference detector is directly

picked up inside the integrating sphere. The second guiding structure, an interface between silica glass and plastic, has its aperture that is very sensitive to temperature, and thus the flux going to the reference photometer increases with temperature (and the ratio shown on Figure 8 decreases).

Once established the correlation, one can correct for it and analyze the resulting photometry. Figure 9 shows the noise properties of the resulting photometry. A noise floor of 25 ppm noise in 6h is reached, this is slightly above the requirement, but the remaining structure in the data seem still corelated to the different temperatures in the lab. Further data reduction might improve this result. In any case this is a clear sign that the limiting factor in the measurement is the test bench and not the instrument.

We had no time to change the fiber and perform and other tests.

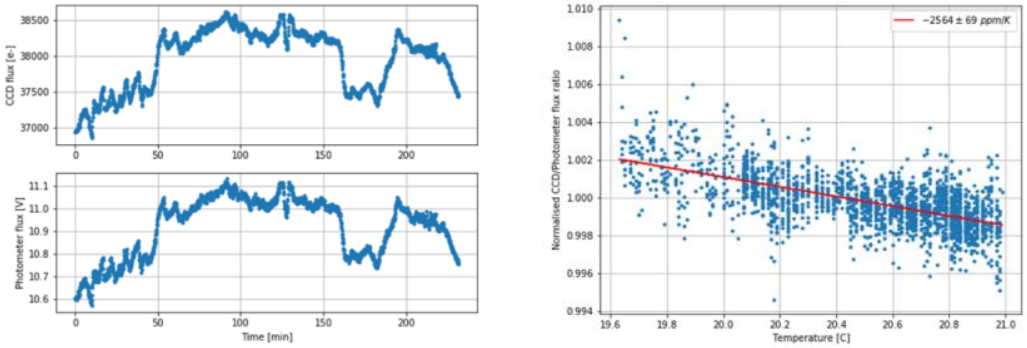

Figure 8 On the left the comparison of the raw flux measured on the instrument and the one of the photometrically stable reference detector of the SSS. On the right the correlation between the lab temperature and the ratio of the flux on the instrument and the one the reference detector.

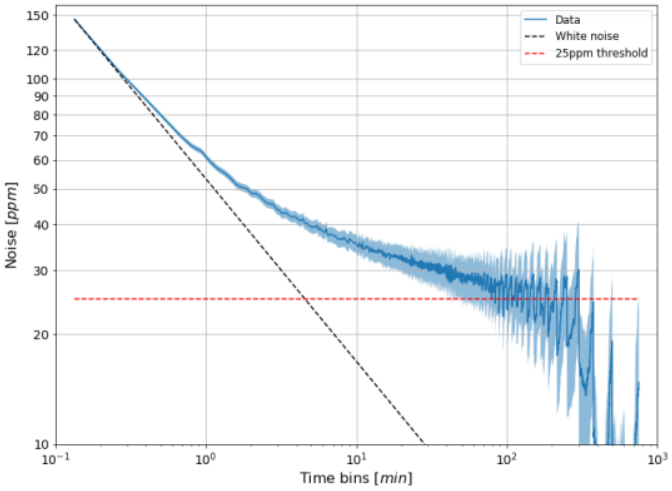

Figure 9 Noise curve computed for the normalized CCD-to-photometer flux ratio. The shaded areas represent the ±1σ-error interval of the curve. The black dashed line shows the slope of a perfect white noise. At a time bin of 6 hours, the noise level has reached a threshold of about 25 ppm, which is likely due to the test set-up and not the instrument.

6. CONCLUSION

We have presented here the results of CHEOPS calibration campaign. We have measured the performances of the detector chain. We have shown in particular that its behavior near to saturation will make it difficult to do saturated star photometry.

The flat-field with a better than 0.1% precision and with the current data it is possible to produce flat-fields adapted to the color of the observed star. We have demonstrated that the instrument intrinsic precision is better than 25 ppm.

REFERENCES

[1] Broeg, C., Fortier, A., Ehrenreich, D., Alibert, Y., Baumjohann, W., Benz, W., Deleuil, M., Gillon, M., Ivanov, A., Liseau, R., Meyer, M., Oloffson, G., Pagano, I., Piotto, G., Pollacco, D., Queloz, D., Ragazzoni, R., Renotte, E., Steller, M., et al., "CHEOPS: A transit photometry mission for ESA's small mission programme," European Physical Journal Web of Conferences **47**, 03005 (2013).

[2] Ricker, G. R., Winn, J. N., Vanderspek, R., Latham, D. W., Bakos, G. Á., Bean, J. L., Berta-Thompson, Z. K., Brown, T. M., Buchhave, L., Butler, N. R., Butler, R. P., Chaplin, W. J., Charbonneau, D., Christensen-Dalsgaard, J., Clampin, M., Deming, D., Doty, J., De Lee, N., Dressing, C., et al., "Transiting Exoplanet Survey Satellite (TESS)," Space Telescopes and Instrumentation 2014: Optical, Infrared, and Millimeter Wave **9143**, 914320 (2014).

[3] Rauer, H., Catala, C., Aerts, C., Appourchaux, T., Benz, W., Brandeker, A., Christensen-Dalsgaard, J., Deleuil, M., Gizon, L., Goupil, M.-J., Güdel, M., Janot-Pacheco, E., Mas-Hesse, M., Pagano, I., Piotto, G., Pollacco, D., Santos, C., Smith, A., Suárez, J.-C., et al., "The PLATO 2.0 mission," Experimental Astronomy **38**, 249–330 (2014).

[4] Wheatley, P. J., West, R. G., Goad, M. R., Jenkins, J. S., Pollacco, D. L., Queloz, D., Rauer, H., Udry, S., Watson, C. A., Chazelas, B., Eigmüller, P., Lambert, G., Genolet, L., McCormac, J., Walker, S., Armstrong, D. J., Bayliss, D., Bento, J., Bouchy, F., et al., "The Next Generation Transit Survey (NGTS)," \mnras **475**, 4476–4493 (2018).

[5] Gillon, M., Jehin, E., Delrez, L., Magain, P., Opitom, C. and Sohy, S., "SPECULOOS: Search for habitable Planets EClipsing ULtra-cOOl Stars," presented at Protostars and Planets VI Posters, 1 July 2013, 2.

[6] Deline, A., Sordet, M., Wildi, F. and Chazelas, B., "The testing and characterization of the CHEOPS CCDs," Society of Photo-Optical Instrumentation Engineers (SPIE) Conference Series **10562**, 105624E (2017).

[7] Wildi, F. P., Chazelas, B., Deline, A., Sordet, M. and Sarajlic, M., "The CHEOPS instrument on-ground calibration system," Techniques and Instrumentation for Detection of Exoplanets VII **9605**, 96051B (2015).

[8] Feline, W. J., "ULTRACAM photometry of eclipsing cataclysmic variable stars," ArXiv e-prints, arXiv:0806.0797 (2008).

[9] Wildi, F. P., Deline, A. and Chazelas, B., "A white super-stable source for the metrology of astronomical photometers," Techniques and Instrumentation for Detection of Exoplanets VII **9605**, 96051T (2015).